ELSEVIER

Journal of Molecular Structure: THEOCHEM 762 (2006) 179–191

THEO CHEM

www.elsevier.com/locate/theochem

Excitation energies from an auxiliary-function formulation of time-dependent density-functional response theory with charge conservation constraint

Andrei Ipatov [a], Antony Fouqueau [a], Carlos Perez del Valle [a], Felipe Cordova [a], Mark E. Casida [a,*], Andreas M. Köster [b], Alberto Vela [b], Christine Jödicke Jamorski [c]

[a] *Équipe de Chimie Théorique, Laboratoire d'Etudes Dynamiques et Structurales de la Sélectivité (LEDSS), UMR CNRS/UJF 5616, Institut de Chimie Moléculaire de Grenoble (ICMG, FR-2607), Université Joseph Fourier (Grenoble I), 301 rue de la Chimie, BP 53, F-38041 Grenoble cedex 9, France*

[b] *Departamento de Química, CINVESTAV, Avenida Instituto Politécnico Nacional 2508, A.P. 14-740 Mexico D.F. 07000, Mexico*

[c] *Laboratorium für Physikalische Chemie, ETH Hoenggerberg, CH-8093 Zürich, Switzerland*

Received 27 June 2005; accepted 18 July 2005
Available online 4 January 2006

Abstract

A key feature of the implementation of density-functional theory (DFT) in many quantum chemistry programs is the use of a charge density fitting (CDF) or resolution-of-the-identity (RI) auxiliary basis. One of these, namely the present-day **deMon2k** (21st century version of *densité de Montréal*) program, makes particularly heavy use of the CDF algorithm. We report the first fully consistent implementation of time-dependent density-functional theory (TDDFT) response theory into the present-day **deMon** code, by which we mean both (i) that the static limit yields analytic derivatives which are correct for the numerical method adapted by **deMon2k** in solving the Kohn–Sham orbital equations and (ii) that the eigenvalue equation appearing in the Casida formulation of TDDFT is properly symmetric. The new implementation is also entirely consistent with using the charge conservation constraint (CCC) in the CDF algorithm. Example calculations on the sodium dimer and tetramer and on *para*-aminobenzonitrile are given showing that the effect of the CCC on TDDFT excitation energies is minor compared to the importance of choosing an adequate auxiliary basis set.

Keywords: Excitation energies; Time-dependent density-functional theory; Charge-density fitting; Resolution-of-the-identity

1. Introduction

Density-functional theory (DFT) provides a formalism for extrapolating to larger molecules the accuracy of highly elaborate correlated ab initio calculations which are presently only possible for smaller molecules. Limitations to the accuracy of DFT quantities come from the need to approximate the exchange–correlation (xc) functional for which no practical exact form is known. Many approximate xc functionals are known and hybrid functionals, which include Hartree–Fock exchange, allow calculations with ab initio-like accuracy to be carried out for molecules at a cost comparable to a Hartree–Fock calculation. Pure density functionals (i.e. those which depend only on the density and not on the orbitals) allow high accuracy for a cost considerably lower than that of a Hartree–Fock calculation, provided that the algorithm which is used can take advantage of the relatively simple multiplicative nature of the xc potential. This might be termed DFt (for 'Density-Functional technology') [1]. One of the most successful of these technologies is that of using a set of charge density fitting (CDF) auxiliary functions. We will show how time-dependent density functional theory (TDDFT) response theory can be implemented in a fully consistent way into a code, namely **deMon2k** (for the 21st century version of *densité de Montréal*), which makes heavy use of the CDF approach. In this way we are completely able to avoid some small inconsistencies which have plagued our earlier work with the **deMon-DynaRho** (**deMon**-dynamic response of the density, ρ) program [2,3].

As is well-known, Hartree–Fock calculations have a formal scaling of $\mathcal{O}(N^4)$ with the number of basis functions, N. This is the number of 4-center electron repulsion integrals (ERIs) over

* Corresponding author. Tel.: +33 4 76 63 56 28; fax: +33 4 76 63 59 83.
E-mail address: mark.casida@ujf-grenoble.fr (M.E. Casida).

0166-1280/$ - see front matter © 2005 Elsevier B.V. All rights reserved.
doi:10.1016/j.theochem.2005.07.034

Table 1
Some index conventions used in this work. The arrows indicate how the functions are abbreviated when bra-ket notation is used

Function	Index type	Notation
Atomic orbitals (AOs)	Greek letters	$\chi_\mu(\vec{r}) \rightarrow \mu$
Molecular orbitals (MOs)	Latin lower case	$\psi_i^\sigma(\vec{r}) \rightarrow i_\sigma$
Auxiliary functions (AFs)	Latin upper case	$f_K(\vec{r}) \rightarrow K$

atomic orbitals (AOs)

$$\langle\mu\nu||\mu'\nu'\rangle = \int\int \chi_\mu(\mathbf{r})\chi_\nu(\mathbf{r})\frac{1}{|\mathbf{r}-\mathbf{r}'|}\chi_{\mu'}(\mathbf{r}')\chi_{\nu'}(\mathbf{r}')\mathrm{d}\mathbf{r}\,\mathrm{d}\mathbf{r}', \quad (1.1)$$

in Mulliken ('charge cloud') notation. The problem remains even for pure DFT because of the classical Coulomb repulsion (Hartree) part of the electronic energy. However, pure DFT may be reduced to a formal scaling of $\mathcal{O}(N^3)$ by the introduction of an auxiliary basis and the use of the resolution-of-the-identity (RI) formula,

$$\hat{1} = \sum_{I,J} ||I\rangle\langle I||J\rangle^{-1}\langle J||, \quad (1.2)$$

where we are using the condensed notation summarized in Table 1 in an abstract bra-ket representation with double bars to indicate the integral metric defined in Eq. (1.1). The action of the right hand side in the position–space representation on an arbitrary auxiliary basis function, f_K, is,

$$\hat{1}f_K(\mathbf{r}) = \sum_{I,J} f_I(\mathbf{r})\langle I||J\rangle^{-1}\langle J||K\rangle = \sum_I f_I(\mathbf{r})\delta_{I,K} = f_K(\mathbf{r}). \quad (1.3)$$

These manipulations, so very simple in appearance, allow the $\mathcal{O}(N^4)$ 4-center ERIs to be expressed in terms of the $\mathcal{O}(N^3)$ 3-center ERIs,

$$\langle\mu\nu||\mu'\nu'\rangle = \sum_I \langle\mu\nu||I\rangle\langle I||J\rangle^{-1}\langle J||\mu'\nu'\rangle. \quad (1.4)$$

The RI strategy has been used as early as the late 1950s [4]. It was used in the early 1970s both in what was to become the modern-day **ADF** (Amsterdam Density Functional) program [5] and in the auxiliary function-based **LCAO-Xα** (Linear Combination of Atomic Orbitals Xα) program of Sambe and Felton [6]. It continues to be used today to simplify Hartree–Fock and other quantum chemistry calculations. For example, Hamel et al. have used the method to help in the calculation of the exact exchange—only Kohn–Sham potential [7–9]. Of particular note in the present context is that the RI strategy is now used in the **Gaussian** [10] and **TurboMol** [11] programs to simplify the Coulomb integrals in DFT calculations. It was also used in the older **DGauss** DFT program [12] and in the **RESTDD** TDDFT program [13,14]. Other uses have been reviewed by Kendall and Früchtl [15].

In reality, the RI approximation is less simple than it first appears. Practical auxiliary basis sets are always incomplete, making

$$\hat{P} = \sum_{I,J} ||I\rangle\langle I||J\rangle^{-1}\langle J||, \quad (1.5)$$

a projector, instead of the identity operator, and making the RI method into an approximation. The quality of the approximation is closely related to the choice of metric. In fact, we could equally well write the resolution-of-the-identity using the simple overlap metric (denoted using a single bar),

$$\hat{1} = \sum_{I,J} |I\rangle\langle I|J\rangle^{-1}\langle J| \qquad \langle\mu\nu|\mu'\nu'\rangle = \int \chi_\mu(\mathbf{r})\chi_\nu(\mathbf{r})\chi_{\mu'}(\mathbf{r})\chi_\nu(\mathbf{r})\mathrm{d}\mathbf{r} \quad (1.6)$$

but the resultant RI approximation using a finite auxiliary basis set has been found, by explicit computation, to be distinctly inferior to that obtained using the Coulomb metric of Eq. (1.5) [16]. The basic reason was first given by Dunlap et al. [17,18] who continued the earlier work of Sambe and Felton [6]. Dunlap introduced the notion of variational fitting of the charge density, ρ. A fit density,

$$\tilde{\rho}(\vec{r}) = \sum_I f_I(\vec{r})x_I, \quad (1.7)$$

was introduced and the CDF coefficients were obtained by minimizing the error

$$\mathcal{E} = \langle\rho-\tilde{\rho}||\rho-\tilde{\rho}\rangle, \quad (1.8)$$

which is equivalent to maximizing the approximate Coulomb repulsion energy, [18,19]

$$\tilde{J} = \langle\tilde{\rho}||\rho\rangle - \frac{1}{2}\langle\tilde{\rho}||\tilde{\rho}\rangle \leq J = \frac{1}{2}\langle\rho||\rho\rangle. \quad (1.9)$$

Minimizing Eq. (1.8) yields the RI approximation with the Coulomb metric,

$$\tilde{\rho}(\vec{r}) = \hat{P}\rho(\vec{r}). \quad (1.10)$$

As Dunlap has emphasized [20], it is the variational nature of this particular RI approximation which accounts for its success.

Strictly speaking, the CDF approach of Dunlap is not the same as the RI approach except at convergence of the self-consistant field (SCF) calculations. This is because the Coulomb energy at the nth SCF iteration is calculated using the fit density obtained from the density of the previous iteration,

$$\tilde{J}^{(n)} = \langle\rho^{(n)}||\tilde{\rho}^{(n-1)}\rangle - \frac{1}{2}\langle\tilde{\rho}^{(n-1)}||\tilde{\rho}^{(n-1)}\rangle \neq J^{(n)} = \frac{1}{2}\langle\rho^{(n)}||\rho^{(n)}\rangle. \quad (1.11)$$

However, the CDF and RI methods do become equivalent at SCF convergence and it is likely that most RI calculations use the CDF approach during the SCF steps.

Dunlap et al. also introduced the notion of a charge conservation constraint (CCC) during the variational fitting,

$$\langle\rho-\tilde{\rho}\rangle = 0, \quad (1.12)$$

where we have introduced the notation (not to be confused with the expectation value of an operator),

$$\langle g\rangle = \int g(\mathbf{r})\mathrm{d}\mathbf{r}. \quad (1.13)$$

This makes sense to the extent that a small error in the number of electrons described by the fit charge density could lead to a chemically significant error in the total energy, and is why the CCC has always been included in the **deMon** programs. This CCC had been introduced sometime before in what was latter to become the **ADF** program [21].

In Section 2 of the paper we will describe our auxiliary function implementation of TDDFT in **deMon2k**.

2. Numerical method

A molecular implementation of TDDFT response theory for the calculation of dynamic polarizabilities and excitation energies has been previously presented by one of us [22]. The fundamental quantities that we need to implement this theory in **deMon2k**, within the TDDFT adiabatic approximation, are analytic derivatives of the appropriate ground state energy within the CDF formalism.

2.1. Elaboration of charge density fitting

The CDF in **deMon2k** makes use of a particular matrix formulation [19] which is easily generalized to any number of constraints, not just the CCC. We first present the generalized version of the CDF here.

The problem to be solved is to minimize the error defined by Eq. (1.8) subject to the constraints,

$$\langle A_i|\tilde{\rho}\rangle = \int A_i(\mathbf{r})\tilde{\rho}(\mathbf{r})\mathrm{d}\mathbf{r} = a_i, \tag{2.1}$$

where once again, we have used the ordinary overlap metric indicated by a single bar. The CCC is just the case where there is a single $A_i(\mathbf{r})$ which is everywhere equal to unity and $a_i = N$, the total number of electrons. *Note that the a_i are taken to be independent of ρ.* It is interesting to note that this resembles the constrained self-consistent field (SCF) idea of Mukerji and Karplus [23] who noted that constraining an SCF calculation to give the experimental value for one property may improve the calculated value of a related property. One could, for example, imagine fixing the value taken by some property in an electronic excited state so as to guide the SCF calculation towards that state [24]. Probably, the most recent application of constrained SCF theory is to the problem of extracting wave functions from X-ray diffraction data [25–29]. Note, however, that true constrained SCF calculations use a constraint on properties calculated from the exact (i.e. orbitally derived) density, $\rho(\mathbf{r})$, while the present CDF method constrains the *fit* density, $\tilde{\rho}(\mathbf{r})$.

The constrained CDF minimization is carried out by the Lagrange multiplier method by minimizing,

$$\begin{aligned} L &= \langle \rho - \tilde{\rho} || \rho - \tilde{\rho}\rangle - 2\sum_i \lambda_i (a_i - \langle A_i|\tilde{\rho}\rangle) \\ 0 &= \frac{\partial L}{\partial x_I} = -2\langle I||\rho\rangle + 2\sum_J \langle I||J\rangle x_J + 2\sum_i \langle I|A_i\rangle \lambda_i, \end{aligned} \tag{2.2}$$

subject to the constraints in Eq. (2.1). This means that we have to solve the simultaneous equations,

$$\begin{aligned} \sum_J \langle I||J\rangle x_J + \sum_i \langle I|A_i\rangle \lambda_i &= \langle I||\rho\rangle \\ \sum_J \langle A_i|J\rangle x_J &= a_i. \end{aligned} \tag{2.3}$$

This can be expressed in matrix notation as,

$$\begin{bmatrix} \mathbf{A} & \mathbf{B} \\ \mathbf{C} & \mathbf{D} \end{bmatrix} \begin{pmatrix} \vec{x} \\ \vec{\lambda} \end{pmatrix} = \begin{pmatrix} \vec{\rho} \\ \vec{a} \end{pmatrix}, \tag{2.4}$$

where

$$\begin{aligned} \mathbf{A} &= \begin{bmatrix} \langle 1||1\rangle & \langle 1||2\rangle & \cdots & \langle 1||M\rangle \\ \langle 2||1\rangle & \langle 2||2\rangle & \cdots & \langle 2||M\rangle \\ \vdots & \vdots & \ddots & \vdots \\ \langle M||1\rangle & \langle M||2\rangle & \cdots & \langle M||M\rangle \end{bmatrix} \\ \mathbf{B} &= \begin{bmatrix} \langle 1|A_1\rangle & \langle 1|A_2\rangle & \cdots & \langle 1|A_m\rangle \\ \langle 2|A_1\rangle & \langle 2|A_2\rangle & \cdots & \langle 2|A_m\rangle \\ \vdots & \vdots & \ddots & \vdots \\ \langle M|A_1\rangle & \langle M|A_2\rangle & \cdots & \langle M|A_m\rangle \end{bmatrix} \\ \mathbf{C} &= \begin{bmatrix} \langle A_1|1\rangle & \langle A_1|2\rangle & \cdots & \langle A_1|M\rangle \\ \langle A_2|1\rangle & \langle A_2|2\rangle & \cdots & \langle A_2|M\rangle \\ \vdots & \vdots & \ddots & \vdots \\ \langle A_m|1\rangle & \langle A_m|2\rangle & \cdots & \langle A_m|M\rangle \end{bmatrix} \\ \mathbf{D} &= \begin{bmatrix} 0 & 0 & \cdots & 0 \\ 0 & 0 & \cdots & 0 \\ \vdots & \vdots & \ddots & \vdots \\ 0 & 0 & \cdots & 0 \end{bmatrix}, \end{aligned} \tag{2.5}$$

and

$$\begin{aligned} \vec{x} &= \begin{pmatrix} x_1 \\ x_2 \\ \vdots \\ x_M \end{pmatrix} \qquad \vec{\lambda} = \begin{pmatrix} \lambda_1 \\ \lambda_2 \\ \vdots \\ \lambda_m \end{pmatrix} \qquad \vec{\rho} = \begin{pmatrix} \langle 1||\rho\rangle \\ \langle 2||\rho\rangle \\ \vdots \\ \langle M||\rho\rangle \end{pmatrix} \\ \vec{a} &= \begin{pmatrix} a_1 \\ a_2 \\ \vdots \\ a_m \end{pmatrix}. \end{aligned} \tag{2.6}$$

By using the fact that, for **A** invertible,

$$\begin{bmatrix}\mathbf{A} & \mathbf{B}\\ \mathbf{C} & \mathbf{D}\end{bmatrix}^{-1} = \begin{bmatrix}\tilde{\mathbf{A}} & \tilde{\mathbf{B}}\\ \tilde{\mathbf{C}} & \tilde{\mathbf{D}}\end{bmatrix}$$
$$\tilde{\mathbf{A}} = \mathbf{A}^{-1} + \mathbf{A}^{-1}\mathbf{B}(\mathbf{D}-\mathbf{C}\mathbf{A}^{-1}\mathbf{B})^{-1}\mathbf{C}\mathbf{A}^{-1} \tag{2.7}$$
$$\tilde{\mathbf{B}} = \mathbf{A}^{-1}\mathbf{B}(\mathbf{D}-\mathbf{C}\mathbf{A}^{-1}\mathbf{B})^{-1}$$
$$\tilde{\mathbf{C}} = -(\mathbf{D}-\mathbf{C}\mathbf{A}^{-1}\mathbf{B})^{-1}\mathbf{C}\mathbf{A}^{-1} \qquad \tilde{\mathbf{D}} = (\mathbf{D}-\mathbf{C}\mathbf{A}^{-1}\mathbf{B})^{-1},$$

that $\mathbf{D}=0$ and that $\mathbf{C}=\mathbf{B}^{\dagger}$, we arrive at the following formulae for the interesting quantities:

$$\vec{\lambda} = (\mathbf{B}^{\dagger}\mathbf{A}^{-1}\mathbf{B})^{-1}\mathbf{B}^{\dagger}\mathbf{A}^{-1}\vec{\rho} - (\mathbf{B}^{\dagger}\mathbf{A}^{-1}\mathbf{B})^{-1}\vec{a}$$
$$\vec{x} = [\mathbf{A}^{-1} - \mathbf{A}^{-1}\mathbf{B}(\mathbf{B}^{\dagger}\mathbf{A}^{-1}\mathbf{B})^{-1}\mathbf{B}^{\dagger}\mathbf{A}^{-1}]\vec{\rho} \tag{2.8}$$
$$-\mathbf{A}^{-1}\mathbf{B}(\mathbf{B}^{\dagger}\mathbf{A}^{-1}\mathbf{B})^{-1}\vec{a}.$$

In principle, the problem of the constrained CDF is now solved. However, it is interesting and informative to rederive the same answer within the abstract vector space spanned by the fitting functions with the Coulomb metric. We immediately face a problem, namely that the observables, $A_i(\mathbf{r})$, are more closely associated, via Eq. (2.1), with the overlap metric than with the Coulomb metric. This is a problem because it means that we are really obliged to work with objects in two distinct metric spaces. However, we can transfer objects from one metric space to the other by a procedure that we shall call embedding. An embedded observable is defined by,

$$\tilde{A}_i(\mathbf{r}) = \sum_{I,J} f_I(\mathbf{r})\langle I||J\rangle^{-1}\langle J|A_i\rangle. \tag{2.9}$$

This has the advantage that,

$$\langle\tilde{A}_i||\tilde{\rho}\rangle = \langle A_i|\tilde{\rho}\rangle = a_i. \tag{2.10}$$

Thus the constrained fit amounts to fixing the lengths of the components of $\tilde{\rho}$ along the various $\tilde{A}_i$ to have appropriate values. This is done with the aid of the projector of Eq. (1.5),

$$\tilde{\rho} = \hat{P}\rho - \sum_j \tilde{A}_j\lambda_j. \tag{2.11}$$

Then

$$a_i = \langle\tilde{A}_i||\tilde{\rho}\rangle = \langle\tilde{A}_i||\rho\rangle - \sum_i\langle\tilde{A}_i||\tilde{A}_j\rangle\lambda_j$$
$$\lambda_j = \sum_i\langle\tilde{A}_j||\tilde{A}_i\rangle^{-1}(\langle\tilde{A}_i||\rho\rangle - a_i)$$
$$||\tilde{\rho}\rangle = \hat{P}||\rho\rangle - \sum_{i,j}||\tilde{A}_j\rangle\langle\tilde{A}_j||\tilde{A}_i\rangle^{-1}(\langle\tilde{A}_i||\rho\rangle - a_i)$$
$$= \left(\hat{P} - \sum_{i,j}||\tilde{A}_j\rangle\langle\tilde{A}_j||\tilde{A}_i\rangle^{-1}\langle\tilde{A}_i||\right)||\rho\rangle - \sum_{i,j}||\tilde{A}_j\rangle\langle\tilde{A}_j||\tilde{A}_i\rangle^{-1}a_i. \tag{2.12}$$

This is the same answer given in Eq. (2.8), albeit in a different form. The quantity in the last parentheses is a new projector,

$$\hat{Q} = \hat{P} - \sum_{i,j}||\tilde{A}_i\rangle\langle\tilde{A}_i||\tilde{A}_j\rangle^{-1}\langle\tilde{A}_j||. \tag{2.13}$$

Finally, it is useful for future use to summarize a few relations involving this projector and the projector $\hat{P}$ of Eq. (1.5),

$$\hat{P}^2 = \hat{P} \quad \hat{Q}\hat{P} = \hat{P}\hat{Q} = \hat{Q} \quad \hat{Q}^2 = \hat{Q}$$
$$\hat{Q}(\rho(\mathbf{r}) - \tilde{\rho}(\mathbf{r})) = 0. \tag{2.14}$$

2.2. Energy expression, Kohn–Sham matrix, and coupling matrices

Having introduced the basic theory of the CDF method with constaints, we may now go on to present the basic DFT equations used in **deMon2k**. Only pure density functionals are used in **deMon2k**, so that the xc energy is only a functional of the spin-up and spin-down charge densities. There are, however, always two different sets of densities in **deMon2k**.

The usual linear combination of atomic orbitals (LCAO) approximation,

$$\psi_{r\sigma}(\mathbf{r}) = \sum_{\mu}\chi_{\mu}(\mathbf{r})c^{\sigma}_{\mu,i}, \tag{2.15}$$

is assumed in **deMon2k** whereby the molecular orbitals (MOs), $\psi_{i\sigma}$, are expressed in terms of atomic orbitals (AOs), χ_{μ}. The spin-σ charge density is,

$$\rho_{\sigma}(\mathbf{r}) = \sum_{i\sigma}\psi_{i\sigma}(\mathbf{r})n_{i\sigma}\psi_{i\sigma}(\mathbf{r}) = \sum_{\mu,\nu}\chi_{\mu}(\mathbf{r})P^{\sigma}_{\mu,\nu}\chi_{\nu}(\mathbf{r}). \tag{2.16}$$

Here, $n_{i\sigma}$ is the occupation number of the MO $\psi_{i\sigma}$ and

$$P^{\sigma}_{\mu,\nu} = \sum_i c^{\sigma}_{\mu,i}n_{i\sigma}c_{\nu,i} \tag{2.17}$$

is the spin-σ density matrix. Of course, we can also talk about the total charge density and total density matrix,

$$\rho(\mathbf{r}) = \rho_{\uparrow}(\mathbf{r}) + \rho_{\downarrow}(\mathbf{r}) \qquad P_{\mu,\nu} = P^{\uparrow}_{\mu,\nu} + P^{\downarrow}_{\mu,\nu}. \tag{2.18}$$

All of these relations concern the *orbital density*.

There is also the *fit density*,

$$\tilde{\rho}_{\sigma}(\mathbf{r}) = \hat{Q}\rho_{\sigma}(\mathbf{r}) - \sum_{i,j}\tilde{A}_i(\mathbf{r})\langle\tilde{A}_i||\tilde{A}_j\rangle^{-1}a_j, \tag{2.19}$$

discussed at length in Section 2.1. Because the fit density is a functional of the orbital density, the fit density is also a function of the density matrix. Its derivative,

$$\frac{\partial\tilde{\rho}_{\sigma}(\mathbf{r})}{\partial P^{\sigma'}_{\nu,\mu}} = \delta_{\sigma,\sigma'}\hat{Q}\chi_{\nu}(\mathbf{r})\chi_{\mu}(\mathbf{r}). \tag{2.20}$$

This is a key equation for what follows.

The usual Kohn–Sham energy expression for a pure density functional is,

$$E = \sum_{i\sigma} n_{i\sigma}\langle\psi_{i\sigma}|\hat{h}|\psi_{i\sigma}\rangle + \frac{1}{2}\langle\rho||\rho\rangle + E_{xc}[\rho_\uparrow, \rho_\downarrow], \tag{2.21}$$

where $\hat{h}$ is the core Hamiltonian, representing the non-interacting kinetic energy and the attraction energy between the electrons and nuclei. The standard approach to DFT in quantum chemistry consists of replacing this expression with

$$E = \sum_{\mu,\nu} h_{\mu,\nu}P_{\nu,\mu} + \frac{1}{2}\langle\rho||\rho\rangle + E_{xc}^{\text{num}}[\rho_\uparrow, \rho_\downarrow], \tag{2.22}$$

where $h_{\mu,\nu} = \langle\mu|\hat{h}|\nu\rangle$ and the superscript on E_{xc}^{num} indicates that matrix elements are to be evaluated by direct numerical integration over a grid in physical (x,y,z) space. This, for example, is the approach used in the program **Gaussian**[10]. The approach taken in **deMon2k** is different.

There are two options in **deMon2k**. The option 'VXCTYPE BASIS' calculates the energy according to the formula,

$$E = \sum_{\mu,\nu} h_{\mu,\nu}P_{\nu,\mu} + \langle\rho||\tilde{\rho}\rangle - \frac{1}{2}\langle\tilde{\rho}||\tilde{\rho}\rangle + E_{xc}^{\text{num}}[\rho_\uparrow, \rho_\downarrow]. \tag{2.23}$$

This method has been around since at least early versions of the **deMon** programs and something very similar can be found as the Coulomb fitting option of **Gaussian**. However, the energy in **deMon2k** may also be calculated using the option 'VXCTYPE AUXIS' according to the expression,

$$E = \sum_{\mu,\nu} h_{\mu,\nu}P_{\nu,\mu} + \langle\rho||\tilde{\rho}\rangle - \frac{1}{2}\langle\tilde{\rho}||\tilde{\rho}\rangle + E_{xc}^{\text{num}}[\tilde{\rho}_\uparrow, \tilde{\rho}_\downarrow]. \tag{2.24}$$

Calculations with the VXCTYPE AUXIS option make full use of the CDF strategy and so are considerably faster than the corresponding calculations with the VXCTYPE BASIS option. In particular, no more than 2-center integrals need to be evaluated numerically, instead of the usual numerical 4-center integrals. To see this more clearly, and for the sake of simplicity, consider the non spin density local density approximation where

$$E_{xc}[\rho] = \int \varepsilon_{xc}(\rho(\mathbf{r}))\rho(\mathbf{r})\mathrm{d}\mathbf{r}. \tag{2.25}$$

Here, $\varepsilon_{xc}(\rho)$ is the xc energy for the homogeneous electron gas with density ρ. When the VXCTYPE BASIS option is used, the density is a linear combination of products of atomic orbitals, $\chi_\mu(\mathbf{r})\chi_\nu(\mathbf{r})$, so that the numerical evaluation of the xc energy involves terms of the form

$$\varepsilon_{xc}\left(\sum_{\mu,\nu}\chi_\mu(\mathbf{r})P_{\mu,\nu}\chi_\nu(\mathbf{r})\right)\chi_{\mu'}(\mathbf{r})\chi_{\nu'}(\mathbf{r}), \tag{2.26}$$

where the four AOs, χ_μ, χ_ν, $\chi_{\mu'}$ and $\chi_{\nu'}$, may be on different centers. In contrast, when the VXCTYPE AUXIS option is used, the density is a linear combination of auxiliary functions, $f_I(\mathbf{r})$, so that the numerical evaluation of the xc energy only involves terms of the form,

$$\varepsilon_{xc}\left(\sum_I f_I(\mathbf{r})x_I\right)f_J(\mathbf{r}), \tag{2.27}$$

which involves only two auxiliary functions, f_I and f_J, on at most two different centers. When spin and dependence on density gradients are taken into account, the reasoning is similar. *Only the VXCTYPE AUXIS option is considered in the present paper.*

The density matrix in Eq. (2.24) is obtained by minimizing the energy subject to the usual orbital orthonormality constraint [30]. This leads to the matrix form of the Kohn–Sham equation,

$$\mathbf{F}^\sigma\vec{c}_{i\sigma} = \varepsilon_{i\sigma}\mathbf{S}\vec{c}_{i\sigma}. \tag{2.28}$$

The quantity,

$$S_{\mu,\nu} = \langle\mu|\nu\rangle, \tag{2.29}$$

is the usual AO overlap matrix. The quantity,

$$F_{\mu,\nu}^\sigma = \frac{\partial E}{\partial P_{\nu,\mu}^\sigma}, \tag{2.30}$$

is the Kohn–Sham matrix. The density-matrix derivative of the energy expression (2.24) is straightforward to carryout with the help of relation (2.20). It gives,

$$F_{\mu,\nu}^\sigma = h_{\mu,\nu} + \langle\mu\nu||\tilde{\rho}\rangle + \langle\hat{Q}\mu\nu||\rho-\tilde{\rho}\rangle + \langle\hat{Q}\mu\nu|v_{xc}^\sigma[\tilde{\rho}_\uparrow, \tilde{\rho}_\downarrow]\rangle, \tag{2.31}$$

where the xc potential,

$$v_{xc}^\sigma[\tilde{\rho}_\uparrow, \tilde{\rho}_\downarrow](\mathbf{r}) = \left[\frac{\delta E_{xc}[\rho_\uparrow, \rho_\downarrow]}{\delta\rho_\sigma(\mathbf{r})}\right]_{\rho_\sigma=\tilde{\rho}_\sigma}. \tag{2.32}$$

However,

$$\langle\hat{Q}\mu\nu||\rho-\tilde{\rho}\rangle = \langle\mu\nu||\hat{Q}(\rho-\tilde{\rho})\rangle = 0, \tag{2.33}$$

because of the last of the relations (2.14). Thus,

$$F_{\mu,\nu}^\sigma = h_{\mu,\nu} + \langle\mu\nu||\tilde{\rho}\rangle + \langle\hat{Q}\mu\nu|v_{xc}^\sigma[\tilde{\rho}_\uparrow, \tilde{\rho}_\downarrow]\rangle. \tag{2.34}$$

It is convenient to introduce the matrix representation of the projector, $\hat{Q}$, namely,

$$\hat{Q} = \sum_{I,J}||I\rangle Q_{I,J}\langle J||, \tag{2.35}$$

where

$$Q_{I,J} = \langle I||J\rangle^{-1} - \sum_{i,j,K,L}\langle I||K\rangle^{-1}\langle K|A_i\rangle\langle\tilde{A}_i||\tilde{A}_j\rangle^{-1}\langle A_j|L\rangle\langle L||J\rangle^{-1}. \tag{2.36}$$

Then

$$\langle v_{xc}^\sigma[\tilde{\rho}_\uparrow, \tilde{\rho}_\downarrow]|\hat{Q}\mu\nu\rangle = \sum_{I,J}\langle v_{xc}^\sigma[\tilde{\rho}_\uparrow, \tilde{\rho}_\downarrow]|I\rangle Q_{I,J}\langle I||\mu\nu\rangle. \tag{2.37}$$

Note that, in the absence of constraints, the fitting procedure just yields,

$$F_{\mu,\nu}^\sigma = h_{\mu,\nu} + \langle\mu\nu||\tilde{\rho}\rangle + \langle\mu\nu||\tilde{v}_{xc}^\sigma[\tilde{\rho}_\uparrow, \tilde{\rho}_\downarrow]\rangle, \tag{2.38}$$

the expected equation for the Kohn–Sham matrix, but using an embedded (or fit) xc potential.

$$v^{\sigma}_{xc}[\tilde{\rho}_{\uparrow},\tilde{\rho}_{\downarrow}] = \sum_{I} f_I(\mathbf{r})\langle I||J\rangle^{-1}\langle I|v^{\sigma}_{xc}[\tilde{\rho}_{\uparrow},\tilde{\rho}_{\downarrow}]\rangle. \tag{2.39}$$

Casida [22] recast basic TDDFT linear response theory in terms of the linear response of the Kohn–Sham density matrix,

$$\delta P_{rs\sigma}(\omega) = \frac{n_{s\sigma}-n_{s\sigma}}{\omega-(\varepsilon_{r\sigma}-\varepsilon_{s\sigma})}\langle\psi_{r\sigma}|\delta v^{\sigma}_{\mathrm{eff}}(\omega)|\psi_{s\sigma}\rangle, \tag{2.40}$$

and the coupling matrix,

$$K^{\sigma,\sigma'}_{\mu\nu,\mu'\nu'} = \frac{\partial^2 E}{\partial P^{\sigma}_{\nu,\mu}\partial P^{\sigma'}_{\nu'\mu'}}. \tag{2.41}$$

Here, the coupling matrix has been expressed in the AO representation, but it is easy to transform to the representation of the unperturbed MOs, which is prefered, at least for formel work. Casida's final result looks very much like the so-called random phase approximation (RPA) used in quantum chemistry. This is usually expressed in terms of the **A** and **B** matrices,

$$\begin{aligned} A_{ia\sigma,jb\tau} &= \delta_{\sigma,\tau}\delta_{i,j}\delta_{a,b}(\varepsilon_{a\sigma}-\varepsilon_{i\sigma}) + K_{ia\sigma,jb\tau} \\ B_{ia\sigma,jb\tau} &= K_{ia\sigma,bj\tau}, \end{aligned} \tag{2.42}$$

where the 'Fortran MO index convention,'

$$\underbrace{abc\ldots fgh}_{\text{unoccupied}}\,\underbrace{|ijklmn|}_{\text{occupied}}\,\underbrace{opq\ldots xyz}_{\text{free}} \tag{2.43}$$

has been introduced. Then

$$\left\{\omega\begin{bmatrix}-1 & 0\\ 0 & 1\end{bmatrix} - \begin{bmatrix}\mathbf{A} & \mathbf{B}\\ \mathbf{B} & \mathbf{A}\end{bmatrix}\right\}\begin{pmatrix}\delta\vec{P}(\omega)\\ \delta\vec{P}^{*}(\omega)\end{pmatrix} = \begin{pmatrix}\Delta\vec{v}_{\mathrm{ext}}(\omega)\\ \Delta\vec{v}^{*}_{\mathrm{ext}}(\omega)\end{pmatrix}, \tag{2.44}$$

where the particle-hole ($ia\sigma$) parts of the applied perturbation and linear response of the Kohn–Sham density-matrix have been represented as column vectors. At an electronic excitation energy, even a small resonance will lead to a discontinuous (i.e. infinite) response of the density matrix. This means that the excitation energies may be determined as the eigenvalues of the pseudo-eigenvalue equation

$$\begin{bmatrix}\mathbf{A} & \mathbf{B}\\ \mathbf{B} & \mathbf{A}\end{bmatrix}\begin{pmatrix}\vec{X}_I\\ \vec{Y}_I\end{pmatrix} = \omega_I\begin{bmatrix}1 & 0\\ 0 & -1\end{bmatrix}\begin{pmatrix}\vec{X}_I\\ \vec{Y}_I\end{pmatrix}, \tag{2.45}$$

which has the classic solution,

$$\begin{aligned} &\mathbf{\Omega}\vec{F}_I = \omega_I^2\vec{F}_I \qquad \mathbf{\Omega} = (\mathbf{A}-\mathbf{B})^{1/2}(\mathbf{A}+\mathbf{B})(\mathbf{A}-\mathbf{B})^{1/2} \\ &\vec{F}_I = (\mathbf{A}-\mathbf{B})^{-1/2}(\vec{X}_I+\vec{Y}_I). \end{aligned} \tag{2.46}$$

In the particular cases of the local and generalized gradient approximations (as opposed to hybrid approximations), the matrix,

$$A_{ia\sigma,jb\tau} - B_{ia\sigma,jb\tau} = \delta_{\sigma,\tau}\delta_{i,j}\delta_{a,b}(\varepsilon_{a\sigma}-\varepsilon_{i\sigma}), \tag{2.47}$$

is particularly simple, making Eq. (2.44) a particularly appealing way to calculate excitation energies from TDDFT.

It remains to establish the form of the coupling matrix for the CDF method with constraints. The coupling matrix used in taking analytic derivatives and in TDDFT is

$$\begin{aligned} K^{\sigma,\sigma'}_{\mu\nu,\mu'\nu'} &= \frac{\partial^2 E}{\partial P^{\sigma}_{\nu\mu}P^{\sigma'}_{\nu'\mu'}} \\ &= \langle\mu\nu||\hat{Q}\mu'\nu'\rangle + \langle\hat{Q}\mu\nu|f^{\sigma,\sigma'}_{xc}[\tilde{\rho}_{\uparrow},\tilde{\rho}_{\downarrow}]|\hat{Q}\mu'\nu'\rangle, \\ &= \langle\hat{Q}\mu\nu||\hat{Q}\mu'\nu'\rangle + \langle\hat{Q}\mu\nu|f^{\sigma,\sigma'}_{xc}[\tilde{\rho}_{\uparrow},\tilde{\rho}_{\downarrow}]|\hat{Q}\mu'\nu'\rangle, \end{aligned} \tag{2.48}$$

where

$$f^{\sigma,\sigma'}_{xc}(\mathbf{r},\mathbf{r}') = \frac{\delta^2 E_{xc}}{\delta\rho_{\sigma}(\mathbf{r})\delta\rho_{\sigma'}(\mathbf{r})}, \tag{2.49}$$

is the xc kernel. Thus the coupling matrix divides into a spin-independent Coulomb (Hartree) part,

$$\langle\hat{Q}\mu\nu||\hat{Q}\mu'\nu'\rangle = \sum_{I,J}\langle\mu\nu||I\rangle Q_{I,J}\langle J||\mu'\nu'\rangle, \tag{2.50}$$

and into a spin-dependent xc part,

$$\langle\hat{Q}\mu\nu|f^{\sigma,\sigma'}_{xc}[\tilde{\rho}_{\uparrow},\tilde{\rho}_{\downarrow}]|\hat{Q}\mu'\nu'\rangle = \sum_{I,J,K,L}\langle\mu\nu||I\rangle Q_{I,J}\langle I|f^{\sigma,\sigma'}_{xc}[\tilde{\rho}_{\uparrow},\tilde{\rho}_{\downarrow}]|J\rangle Q_{J,K}\langle K||\mu'\nu'\rangle. \tag{2.51}$$

Note that the RI-2 approximation in the **RESTDD** program [14] is obtained from these last two equations by replacing $Q_{I,J}$ with $\langle I||J\rangle^{-1}$, that is by neglect of the fitting constraints. However, what is particularly interesting is that this equation is introduced in **RESTDD** as an additional approximation to help in solving Casida's equation, without regard to consistence with approximations in the pre-**RESTDD** self-consistent field program used (**PARAGAUSS**). Here, of course, we have taken special care that the response equations are completely consistant with both the self-consistent field Kohn–Sham equations solved and with the initial DFT energy expression used. This has the important advantage that Casida's equation may eventually be used to calculate excited state analytic derivatives without any fear of inconsistencies.

This completes our explanation of the methodology used in this paper. The method is, of course, very general. Even without the inclusion of constraints, this numerical approach is a distinct improvement over what had been done previously in **deMon-DynaRho**. In the initial version of **deMon-DynaRho**[2], we were careful that the coupling matrix elements corresponded to the second derivatives of the energy expression used in **deMon-KS**[31]. That guaranteed that the static polarizability calculated as the static limit of the TDDFT polarizability was the correct analytic derivative quantity. However, the coupling matrix was not exactly symmetric and this lead to difficulties in calculating nearly degenerate

excitation energies [2]. That is why a later version of **deMon-DynaRho** used the numerical method proposed in Ref. [3] where the coupling matrix is symmetric but the static limit of TDDFT no longer gave the exact analytic derivatives. In the numerical method described here and now implemented, the coupling matrix is symmetric (and in fact resembles that described in Ref. [3]) *and* the static limit of TDDFT is the exact analytic derivative for the appropriate energy expression. Thus certain small but irritating inconveniences which plagued the TDDFT implementation in **deMon-DynaRho** have been overcome in a new elegant formalism.

In the remainder of the paper, we will illustrate how this new method compares with an auxiliary function-free method, in particular giving an idea of what quality of results can be expected from different auxiliary basis sets. But our real interest is in the utility (or lack thereof) of the CCC for calculating TDDFT excitation energies. Thus we will confine our calculations to the case of the CCC—that is, the case of a single A_i which is equal to unity.

3. Computational details

The **deMon** series of programs dates back to code first developed at the University of Montreal in the mid-1980 s, during the course of Alain St-Amant's Ph.D. thesis. Suffice it to say that the **deMon** programs share a common philosophy of using Gaussian-type orbital and auxiliary basis sets. Exchange-correlation integrals are evaluated by direct numerical integration over a Becke-type grid. Details of the original implementation may be found in Alain St-Amant's thesis (in French). In the mid-1990s, Casida described the molecular implementation of TDDFT [22], which has now been adapted in a most widely used quantum chemistry programs. The initial **deMon** impementation of the Casida equations appeared as **deMon-DynaRho** [32], a post-**deMon-KS** [31] program. The first calculations with **deMon-DynaRho** were reported in Refs. [33] and [2]. Improved numerical methodology was described in Ref. [3] and subsequently implemented in **deMon-DynaRho**. The original **deMon-KS** of Alain St-Amant's PhD thesis has undergone many evolutions. It was finally decided to rewrite the entire program making numerous algorithmic improvements. The result is **deMon2k**[34].

Only the most recent version of **deMon2k** includes TDDFT. It is to be emphasized here that our object is to make a new more efficient auxiliary function-based implementation of TDDFT whose finite orbital and auxiliary-function formalism are as trustworthy a reflection as possible of the formal properties of the formally exact Casida equations [22], in the sense of having symmetric matrices and reducing to true analytic derivatives for the appropriate underlying energy expressions. Our initial modifications of **deMon-DynaRho** to make it a post-SCF program for **deMon2k** gave reasonable answers but did not completely meet our objective. That is why the numerical method for TDDFT described in this paper has been incorporated directly into the heart of **deMon2k**. This implementation is so far only partial in so far as some of the desirable features of **deMon-DynaRho** have yet to be

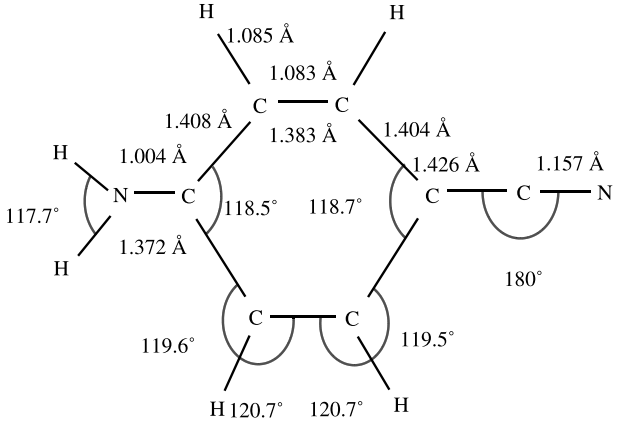

Fig. 1. Planar C_{2v} geometry used in our pABN calculations.

transfered to the new program and calculations are limited to the adiabatic local density approximation (also called the time-dependent local density approximation). These are, of course, temporary limitations which will disappear in the normal course of development of **deMon2k**.

Test calculations were carried out on Na_2, Na_4 and *para*-aminobenzonitrile (pABN). The geometry used for pABN is the symmetric planar geometry shown in Fig. 1, which is close to what is obtained from a DFT calculation with the B3LYP functional. The geometries used for the sodium clusters are shown in Fig. 2. They have been obtained with the program **Gaussian** [10] using the B3LYP functional and the Sadlej basis set [35]. The orbital basis sets used in all calculations reported here are the Sadlej basis sets[35] which were designed to describe polarizabilities (rather than excitation energies) but which are adequate for present purposes.

Most calculations were carried out with the MEDIUM grid, though some calculations were carried out with the FINE grid. The **deMon2k** program has the option to use an adaptive grid which adds grid points until a predetermined accuracy is obtained in the integration of the charge density. Tests showed that the CCC lead to the use of different adaptive grids and hence somewhat uncontrolled comparisons. We have, therefore, decided to avoid the use of adaptive grids in the calculations reported here.

Several different auxiliary basis sets were used. The GEN-A*n* and GEN-A*n**, $n = 1$, 2, or 3, auxiliary basis sets are generated

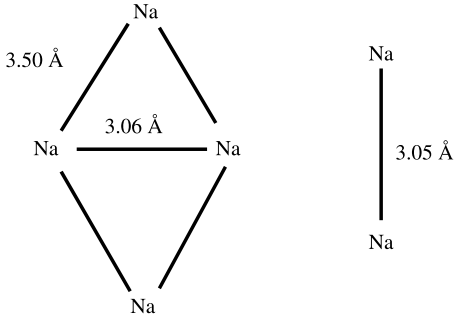

Fig. 2. Na cluster geometries used in our calculations. Symmetries: Na_2 $D_{\infty h}$, Na_4 $D_{4\,h}$.

automatically by the **deMon2k** program based upon the orbital basis set coefficients. Auxiliary functions are grouped into *s*, *spd*, and *spdfg* sets with shared exponents. The GEN-A*n* basis sets make use of the *s* and *spd* groups, while the GEN-A*n** also uses *spdfg* groups. The exponents are determined by the smallest and largest primitive Gaussian exponents in the orbital basis set via an essentially even tempered progression [36,37]. The larger the value of *n* the better the coverage of the auxiliary function space, so the quality of the auxiliary basis sets increase in going from A1 to A2 to A3. The exact procedure is described in **deMon2k** manual.

Comparisons were made against **Gaussian**[10] TDDFT calculations using the same geometry and orbital basis sets, but without the use of auxiliary basis functions. That is, the charge density fitting option in **Gaussian** was *not* used and no approximation took place for the 4-center integrals.

4. Results

We wanted to answer two related questions here. The first is to obtain an idea of the quality of auxiliary basis set necessary to get converged answers for TDDFT excitation energies and oscillator strengths. We also wanted to determine the importance (or lack thereof) of the CCC. The fit density is used in **deMon2k** in calculating the Coulomb (Hartree) and xc contributions to the orbital hamiltonian and total energy. It is logical to think that a small error in the charge density would lead to small errors in the orbital hamiltonian and total energy, which would nevertheless be large on the scales of spectroscopic and chemical accuracy. Indeed it has been found that the inclusion of the CCC increases the accuracy of the electron number obtained by total numerical integration of the orbital density by at least an order of magnitude. It is reasonable to think that excitation energies and oscillator strengths would also benefit from the CCC by reducing the size of the auxiliary-basis set needed for a given level of convergence. We decided to test this hypothesis with calculations on *para*-aminobenzonitrile (pABN) and some small sodium clusters. This choice was partly governed by our own prior experience with these types of systems [40–58], but also makes sense in that the physics and chemistry of these two types of systems is very different. The excitation energies considered are all well below the TDLDA ionization threshold at minus the highest occupied molecular orbital energy (see Table 2.)

Table 2
Ionization potentials for molecules treated in this work

Na excitation energies (eV)			
Molecule	$-\varepsilon_{HOMO}$[a]	ΔSCF[b]	Expt[c]
Na_2	3.56	5.25	4.93
Na_4	3.00	4.30	4.27
pABN	6.25	8.16	8.17

[a] The negative of the highest occupied molecular orbital energy, present work.
[b] The ΔSCF ionization potential, present work.
[c] Experimental values for sodium clusters from Ref. [38]. Experimental value for pABN from Ref. [39].

Even for most of these molecules, full diagonalization of the TDLDA method is not possible and the block Davidson Krylov space method is usually used to find the lowest 20 or so excitations. Thus this molecule is also a test of the **deMon2k** block Davidson procedure which showed no particular problems.

TDLDA calculations were performed both with and without the charge conservation constraint (CCC) in the SCF and/or TDDFT steps with 5 different auxiliary basis sets.

4.1. Small sodium clusters

To a first approximation, the electronic structure of even very small sodium clusters is relatively well described by the shell model [59]. In this model, the cluster is thought of as an elipsoidal jellium droplet, filled with the valence electrons in a harmonic oscillator-type potential. The shape of the cluster can be obtained by varying the major axes of the elipsoid so as to minimize the total energy. That the nuclei arrange themselves to minimize the energy of the electrons, instead of the electrons arranging themselves to minimize the nuclear repulsions, may be considered as evidence of metallic rather than covalent bonding. In any event, the harmonic oscillator aspect of the shell model implies that there should be three major electronic transitions corresponding to the harmonic modes along each of the three different axes. Should these axes be degenerate (as is the case for cylindrically symmetric diatomics), even fewer major transitions will be observed.

The shell model predicts two principle excitations for Na_2: a non degenerate $\Sigma_u^+(\sigma_g \rightarrow \sigma_u)$ excitation and a degenerate $\Pi_u(\sigma_g \rightarrow \pi_u)$ excitation. In practice the two Π_u excitations are not exactly degenerate in our calculations because of very slight symmetry breaking which occurs due to the use during the numerical integration steps of the calculation of a grid whose symmetry is not strictly identical to that of the molecule. This effect is, however, very small. Our TDLDA results are compared with experiment and ab initio results in Table 3. The TDLDA somewhat overestimates the excitation energies of the two singlet states.

Numerical errors in our calculated excitation energies and oscillator strengths are shown in Figs. 3 and 4. As expected, the errors in calculated excitation energies and oscillator strengths decreases, albeit non-monotonically, as the quality of the auxiliary basis set increases. The most accurate work requires

Table 3
Comparison of our TDLDA excitation energies with experimental and ab initio results from the literature

Na_2 excitation energies (eV)[a]					
Excitation	Expt[a]	TDLDA[b]	FCI[c]	CI[d]	MBPT[e]
$^1\Sigma_+^u$	1.820	2.10	1.928	1.823	1.627
$^1\Pi_u$	2.519	2.64	2.576	2.517	2.572

[a] As cited in Ref. [60].
[b] Present work.
[c] Full configuration interaction [61].
[d] Configuration interaction [62].
[e] Many-body perturbation theory [63].

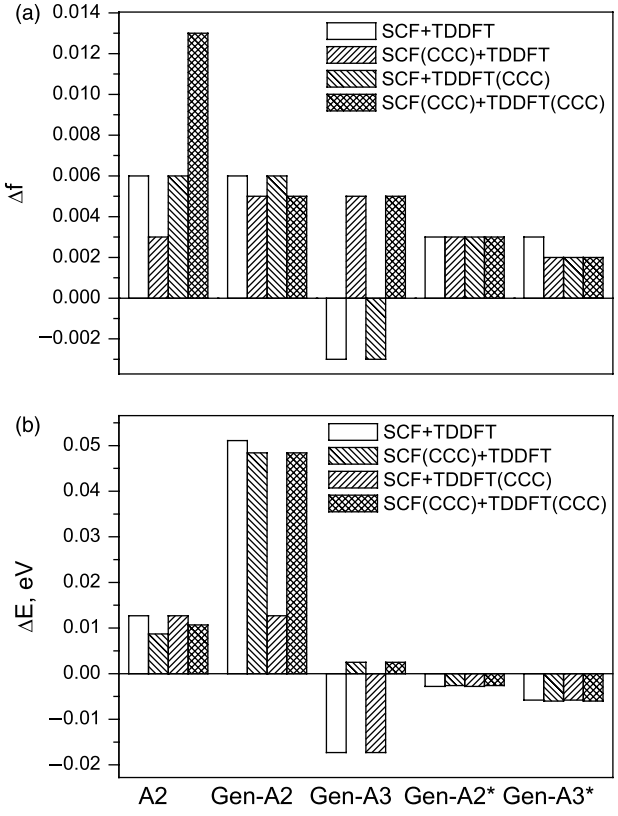

Fig. 3. Errors in the Na_2 $^1\Sigma_+^u$ excitation (2.10 eV) as a function of algorithm and auxiliary basis set: bottom energy, top oscillator strength.

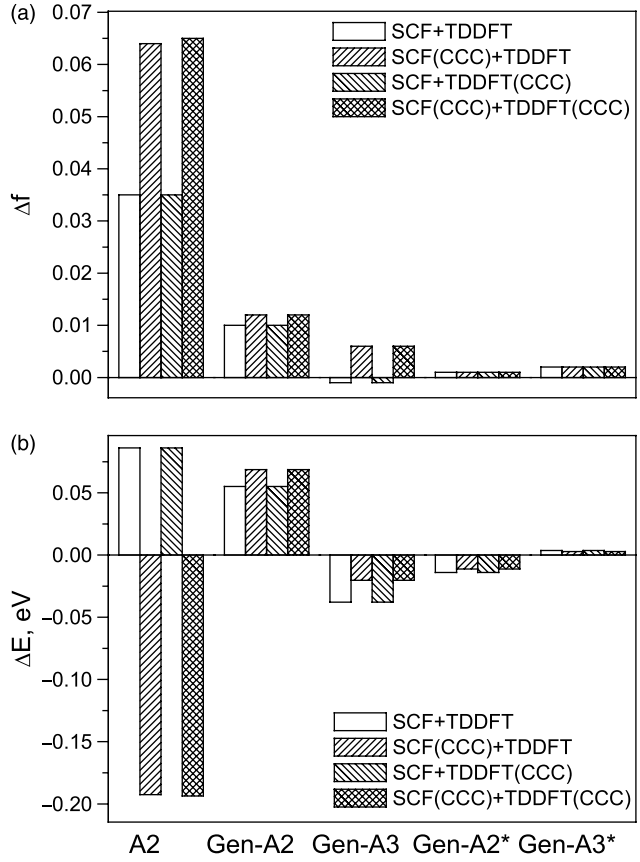

Fig. 4. Errors in Na_2 $^1\Pi_u$ excitation (2.64 eV) as a function of algorithm and auxiliary basis set: bottom energy, top oscillator strength.

the inclusion of polarization functions in the auxiliary basis set. Maximal errors of less than 0.02 eV in the excitation energies are obtained with the Gen-A2* and Gen-A3* auxiliary basis sets. Perhaps most remarkable is that, apart from a few exceptions, it is the use or non use of the CCC in the pre-TDDFT SCF calculation rather than in the post-SCF TDDFT which determines the size of the errors in the excitation energies and oscillator strengths. It is difficult to say if the CCC aids convergence with respect to the quality of the auxiliary basis set. However, the CCC involves little computational overhead and does not markedly deteriorate the quality of the calculated excitation energies and oscillator strengths.

For Na_4, the shell model predicts three principle absorptions. As indicated in Table 4, this is indeed what is reported in the literature. Our tests concentrated on the four lowest singlet excitations, only one of which belongs to the three principle absorptions predicted by the shell model. Numerical errors for these four lowest singlet excitations are given in Figs. 5 and 6. Our conclusions are essentially identical to those already drawn for the dimer calculations. Increasing the quality of the auxiliary basis set decreases on average the size of the numerical error in the excitation energy. The Gen-A3* auxiliary basis set is able to give excitation energies to within 0.02 eV of those calculated using the **Gaussian** program without charge density fitting. Here, even more than in the case of the dimer, the size of the errors are determined almost exclusively by whether or not the CCC has been used in the SCF step.

4.2. *para*-Aminobenzonitrile

pABN is a classic example of a push–pull chromophore which has a strong charge transfer excitation (Fig. 7). Such polymers can be attached to polymer backbones and aligned in an electric field to obtain Langmuir–Blodget films with important nonlinear optical properties [66]. In particular, as a first approximation, the second hyperpolarizability is often

Table 4
Comparison of our TDLDA Na_4 excitation energies with experimental and ab initio results from the literature

Na excitation energies (eV)			
Excitation	Expt[a]	TDLDA[b]	MRD-CI[c]
1^1B_{2u}	1.63	1.49	1.51
1^1B_{3u}[d]	1.80	1.81	1.71
2^1B_{3u}	1.98	2.03	1.87
1^1B_{1u}	2.18	2.24	2.07
3^1B_{2u}[d]	2.51	2.57	2.45
2^1B_{1u}[d]	2.78	2.76	2.76

[a] From Ref. [64].
[b] Present work.
[c] Multireference doubles configuration interaction [65].
[d] Principle peaks corresponding expected from the shell model and found in the MRD-CI calculations of Ref. [65].

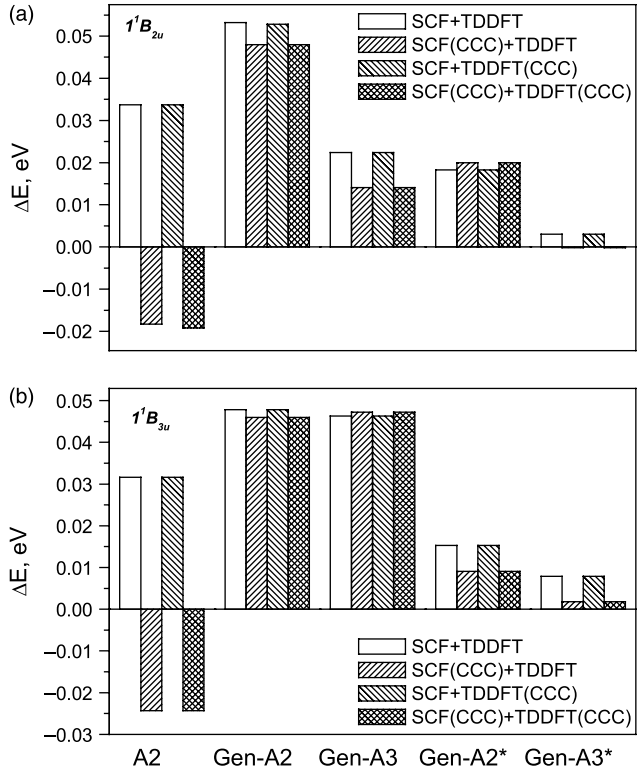

Fig. 5. Errors in the Na_4 1^1B_{2u} (1.49 eV) and 1^1B_{3u} (1.81 eV) excitations as a function of algorithm and auxiliary basis set.

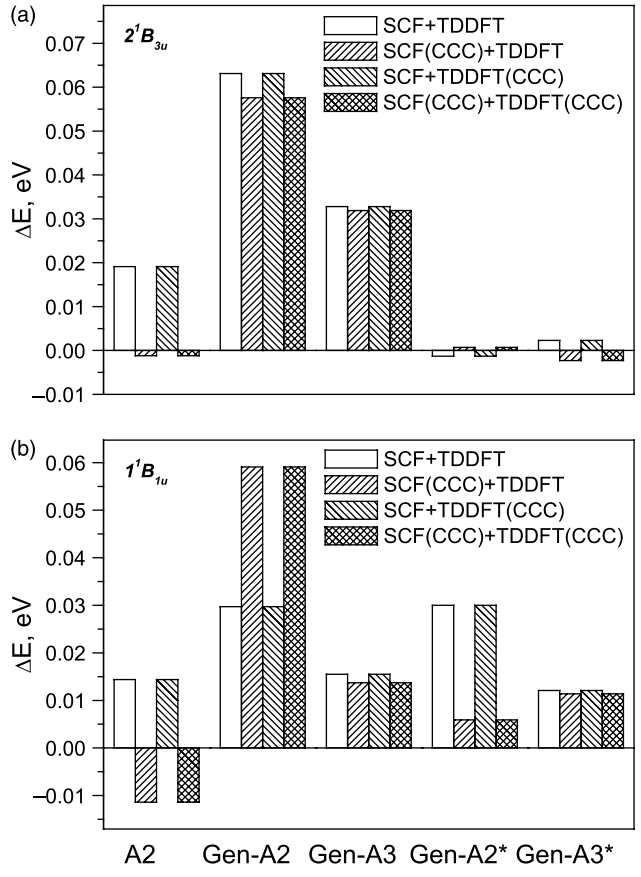

Fig. 6. Errors in $Na_4 2^1B_{3u}$ (2.03 eV) and 1^1B_{1u} (2.24 eV) excitations as a function of algorithm and auxiliary basis set.

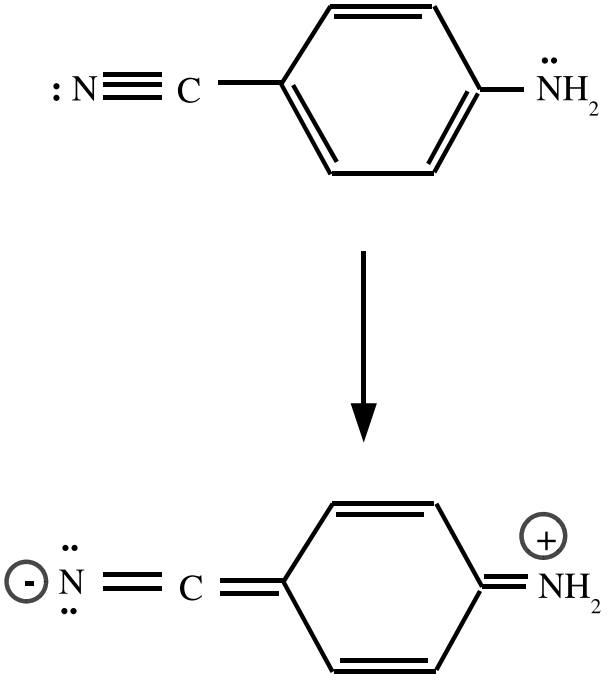

Fig. 7. Traditional picture of the photoexcited charge transfer state in pABN.

described in terms of this one excitation,

$$\beta(\omega) \propto \frac{\mu\omega_{CT} f_{CT}\Delta\mu}{(\omega_{CT}^2-\omega^2)(\omega_{CT}^2-4\omega^2)}, \tag{4.1}$$

where ω_{CT} is the charge transfer excitation energy, f_{CT} is the corresponding oscillator strength, μ is the groundstate dipole

Table 5
Previous results for ABN vertical singlet excitations

Vertical excitations (eV)	
Method	Excitation energy (Oscillator strength)
^{1}B(LE,HOMO→LUMO)	
Expt.[a]	4.2
CASPT2[b]	4.01 (0.00)
CASPT2[c]	4.09
TD-LDA/6-31G*[c]	~4.25
TD-LDA[d]	4.21 (0.02)
TD-B3LYP[c]	4.58
TD-B3LYP[d]	4.57 (0.02)
CS-INDO[e]	4.08
^{1}(CT,HOMO→LUMO+1)	
Expt.[a]	4.7
CASPT2[b]	4.44 (0.36)
CASPT2[c]	4.45
TD-LDA/6-31G*[c]	~4.70
TD-LDA[d]	4.61 (0.39)
TD-B3LYP/6-31G*[c]	4.89
TD-B3LYP[d]	5.06 (0.40)
CS-INDO[e]	4.67

[a] As given in Table 2 of Ref. [52].
[b] L. Serrano-Andres et al. [68]. Oscillator strengths are calculated at the CASSCF level.
[c] F. Gutierrez, PhD thesis [67].
[d] Calculations denoted (Sm/Bg) in Table 2 of Ref. [52].
[e] A. Germain, PhD thesis [69].

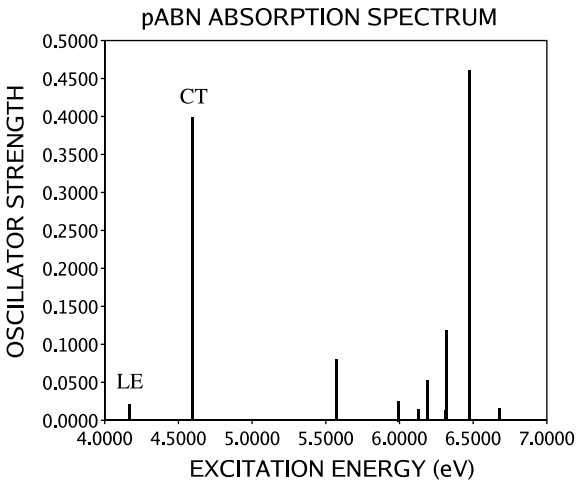

Fig. 8. pABN TDLDA spectrum calculated using the Sadlej basis set and Fine grid.

moment, and $\Delta\mu$ is the change in the dipole moment upon excitation (e.g. Ref. [66] p. 54). pABN and related molecules also show an interesting double florescence phenomenon which has been studied using TDDFT by Gutierrez [67] and especially by Jamorski and coworkers [52–58]. Results from previous work are shown in Table 5. Our calculated TDLDA spectrum for pABN is given in Fig. 8. The first excitation at about 4.15 eV is the so-called local excitation (LE) corresponding to the highest occupied molecular orbital

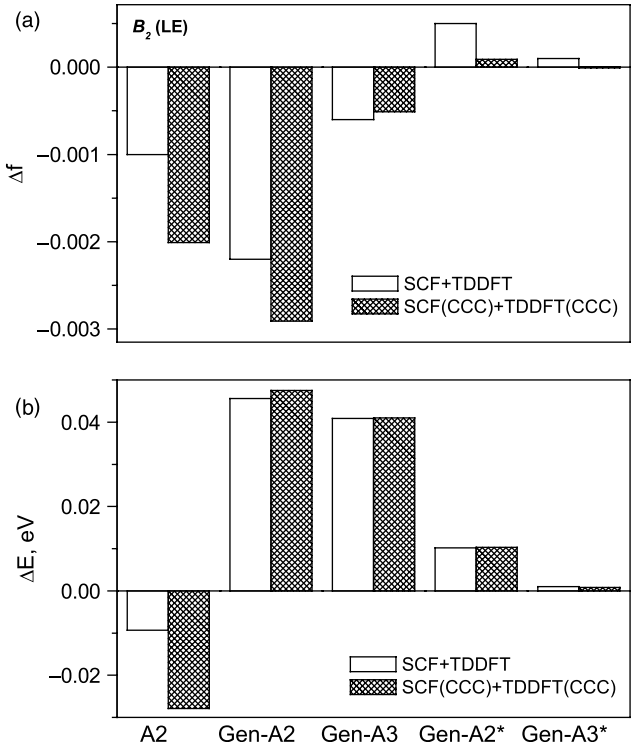

Fig. 9. Errors in the pABN singlet local excitation (LE) energy (4.12 eV) as a function of algorithm and auxiliary basis set: bottom energy, top oscillator strength.

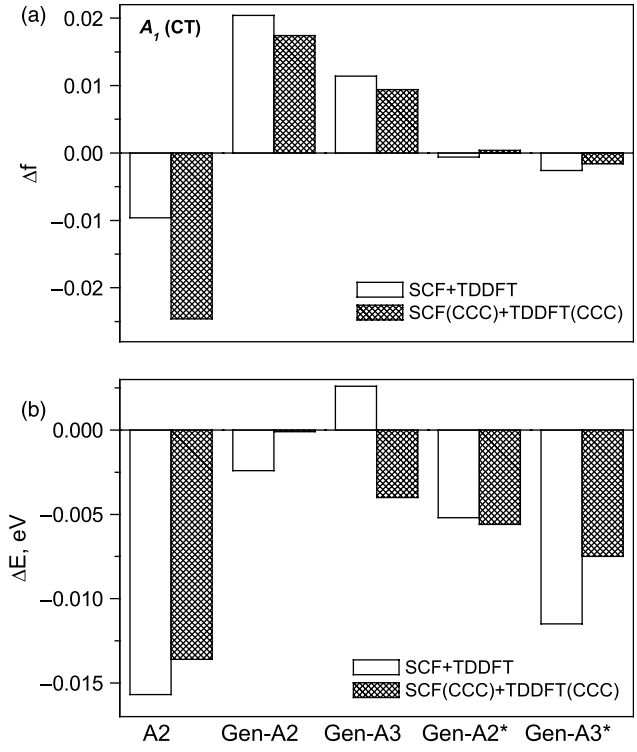

Fig. 10. Errors in the pABN singlet local excitation (CT) energy (4.60 eV) as a function of algorithm and auxiliary basis set: bottom energy, top oscillator strength.

(HOMO) to lowest unoccupied molecular orbital (LUMO) singlet excitation. The charge transfer (CT) excitation is at about 4.7 eV and corresponds to the HOMO→LUMO+1.

Numerical errors in the singlet transition energies for different auxiliary basis sets are shown in Fig. 9 for the LE excitation and in Fig. 10 for the CT excitation. We have already seen in our sodium cluster calculations that the size of the error in our excitation energies is dominated by whether or not the CCC is used at the SCF step. For this reason only calculations consistantly using or neglecting the CCC at both the SCF and TDDFT steps have been shown. Excitation energy errors are below or about 0.02 eV with use of the GEN-A2* or GEN-A3* auxiliary basis sets.

5. Conclusion

Many quantum chemists think of density-functional theory (DFT) as a Hartree–Fock (HF) like theory which includes some electronic correlation through the use of an approximate exchange–correlation functional. If we restrict ourselves to this point of view, we should expect DFT to give better results than HF calculations for a similar amount of computational effort. Indeed, this is what is typically found since many quantum chemistry codes continue to evaluate 4-center integrals. However, pure DFT (as opposed to hybrid methods) is a Hartree-like, rather than a HF-like method, in so far as the self-consistent field is described by a purely multiplicative potential

(v_{xc}). That means that a properly implemented DFT should give results comparable to correlated ab initio methods, but for *less* effort than a HF calculation. This is made possible in the **deMon2k** program by using auxiliary functions and the charge density fitting (CDF) method to completely eliminate 4-center integrals, replacing them with at most 3-center integrals. In the case of those integrals which have to be evaluated numerically, the VXCTYPE AUXIS option avoids the numerical evaluation of more than 2-center integrals, yielding a substantial reduction of computational effort. In this paper, we have extended the CDF strategy to include TDDFT and report results of our implementation in **deMon2k**.

The equations are general for a constrained CDF. Philosophically, this is similar to the constrained SCF idea of Mukherji and Karplus [23] who reported that calculated properties could be improved if SCF calculations were constrained to give the experimental values of related properties. This is a subtle idea which implicitly assumes that the properties of interest depend on regions of configuration space which have a relatively low energetic weighting and so are unlikely to be completely fixed by a variational minimization.

Only a charge conservation constraint (CCC) was imposed upon our fit density in our calculations. In lines with the ideas of Mukherji and Karplus, the CCC is found to increase by an order of magnitude the precision of the electron number obtained by direct numerical integration of the orbital density. Comparisons between our **deMon2k** TDDFT excitation energies and oscillator strengths, and those obtained from Gaussian without the use of auxiliary basis function methodology, indicate that inclusion of the CCC may or may not have value for TDDFT calculations. What is clear cut is that the CCC affects the SCF part of the calculation more than the TDDFT part of the calculation and that the effect is small. Also clear is that the choice of a good auxiliary basis set is more important than the CCC. In terms of Mukherji and Karplus' idea, the total electron number is probably adequately determined for subsequent TDDFT calculations by the initial SCF calculation, and so it is not an especially important property to constrain when considering excitation spectra. On the otherhand, inclusion of the CCC involves only a small additional computational cost and leads to a fully consistent method which may also be applied to properties which are more sensitive to the the CCC.

Overall, the major advantage of the present method is that it is simultaneously efficient and yet satisfies key properties of the exact TDDFT equations. That is, the coupling matrix is manifestly symmetric, as it should be, and the static limit of TDDFT gives proper analytic derivatives of the appropriate energy expression. This means that we have a schema which allows TDDFT to be fully integrated within the **deMon2k** code without modification of the underlying **deMon2k** numerical approximations and which will allow the method to form an essential building block for the calculation of excited-state analytical derivatives at some point in the future.

Acknowledgment

It is a pleasure to dedicate this paper to Annick Goursot on the occasion of her sixtieth birthday. Annick was one of the first theoretical chemists in France to make broad use of DFT. MEC, CJJ, AV, and AK came to know Annick through her involvement in the development of the **deMon** suite of DFT programs. For this reason, it seems particularly meaningful to us to be able to dedicate a paper to her volume on a methodological subject concerning DFT and, in particular, **deMon**.

This study was carried out in the context of a Franco-Mexican collaboration financed through *ECOS-Nord* Action M02P03. It has also benefited from participation in the French *groupe de recherche en density functional theory* (DFT) and the European working group COST D26/0013/02. Those of us at the Université Joseph Fourier would like to thank Pierre Vatton, Denis Charapoff, Régis Gras, Sébastien Morin, and Marie-Louise Dheu-Andries for technical support of the LÉDSS and *Centre d'Expérimentation pour le Calcul Intensif en Chimie* (CECIC) computers used for the calculations reported here. AF would like to thank the French *Ministère d'Education* for a *Bourse de Mobilité*. CP and AI would like to acknowledge funding from LÉDSS during their postdoctoral work. (An early part of this work was performed by CP as a postdoc before he obtained a permanent position in the LÉDSS.) The LÉDSS funded a 1 month working visit for CJJ in 2002. FC acknowledges support from the Mexican Ministry of Education via a CONACYT (SFERE 2004) scholarship and from the Universidad de las Americas Puebla (UDLAP). We would also like to thank Jean-Pierre Daudey and Fabien Gutierez for interesting discussions concerning the spectrocopy of aminobenzonitrile. Roberto Flores is also thanked for many useful discussions.

References

[1] Term proposed by the late Jan Almlöf.
[2] C. Jamorski, M.E. Casida, D.R. Salahub, J. Chem. Phys. 104 (1996) 5134.
[3] M.E. Casida, in: J.M. Seminario (Ed.), Recent Developments and Applications of Modern Density Functional Theory, Elsevier, Amsterdam, 1996, p. 391.
[4] S.F. Boys, I. Shavitt, University of Wisconsin, Report WIS-AF-13, 1959.
[5] E.J. Baerends, D.E. Ellis, P. Ros, Chem. Phys. 2 (1973) 41.
[6] H. Sambe, R.H. Felton, J. Chem. Phys. 62 (1975) 1122.
[7] S. Hamel, M.E. Casida, D.R. Salahub, J. Chem. Phys. 114 (2001) 7342.
[8] S. Hamel, M.E. Casida, D.R. Salahub, J. Chem. Phys. 116 (2002) 8276.
[9] S. Hamel, P. Duffy, M.E. Casida, D.R. Salahub, J. Electron. Spectrosc. 123 (2002) 345.
[10] M.J. Frisch, G.W. Trucks, H.B. Schlegel, G.E. Scuseria, M.A. Robb, J.R. Cheeseman, J.A. Montgomery, Jr., T. Vreven, K.N. Kudin, J.C. Burant, J.M. Millam, S.S. Iyengar, J. Tomasi, V. Barone, B. Mennucci, M. Cossi, G. Scalmani, N. Rega, G.A. Petersson, H. Nakatsuji, M. Hada, M. Ehara, K. Toyota, R. Fukuda, J. Hasegawa, M. Ishida, T. Nakajima, Y. Honda, O. Kitao, H. Nakai, M. Klene, X. Li, J.E. Knox, H.P. Hratchian, J.B. Cross, V. Bakken, C. Adamo, J. Jaramillo, R. Gomperts, R.E. Stratmann, O. Yazyev, A.J. Austin, R. Cammi, C. Pomelli, J.W. Ochterski, P.Y. Ayala, K. Morokuma, G.A. Voth, P. Salvador, J.J. Dannenberg, V.G. Zakrzewski, S. Dapprich, A.D. Daniels, M.C. Strain, O. Farkas, D.K. Malick, A.D. Rabuck, K. Raghavachari, J.B. Foresman, J.V. Ortiz, Q.

Cui, A.G. Baboul, S. Clifford, J. Cioslowski, B.B. Stefanov, G. Liu, A. Liashenko, P. Piskorz, I. Komaromi, R.L. Martin, D.J. Fox, T. Keith, M.A. Al-Laham, C.Y. Peng, A. Nanayakkara, M. Challacombe, P.M.W. Gill, B. Johnson, W. Chen, M.W. Wong, C. Gonzalez, J.A. Pople, GAUSSIAN 03, Revision C.02, Gaussian, Inc., Wallingford CT, 2004.
[11] R. Bauernschmitt, M. Häser, O. Treutler, R. Ahlrichs, Chem. Phys. Lett. 264 (1997) 573.
[12] J. Andzelm, in: J. Labanowski, J. Andzelm (Eds.), Density Functional Methods in Chemistry, Springer, New York, 1991, p. 155.
[13] A. Görling, H.H. Heinze, S.Ph. Ruzankin, M. Staufer, N. Rösch, J. Chem. Phys. 110 (1999) 2785.
[14] H.H. Heinze, A. Görling, N. Rösch, J. Chem. Phys. 113 (2000) 2088.
[15] R.A. Kendall, H.A. Früchtl, Theor. Chem. Acc. 97 (1997) 158.
[16] O. Vahtras, J. Almlöf, M.W. Feyereisen, Chem. Phys. Lett. 312 (1993) 514.
[17] B.I. Dunlap, J.W.D. Connolly, J.R. Sabin, J. Chem. Phys. 71 (1979) 3396.
[18] B.I. Dunlap, J.W.D. Connolly, J.R. Sabin, J. Chem. Phys. 71 (1979) 4993.
[19] A.M. Köster, P. Calaminici, Z. Gómez, U. Reveles, in: K.D. Sen (Ed.), Reviews of Modern Quantum Chemistry, World Scientific, Singapore, 2002, p. 1439.
[20] B.I. Dunlap, Phys. Chem. Chem. Phys. 2 (2000) 2113; B.I. Dunlap, J. Mol. Struct.: THEOCHEM 501–502 (2000) 221; B.I. Dunlap, J. Mol. Struct.: THEOCHEM 529 (2000) 37.
[21] E.J. Baerends, P. Ros, Int. J. Quant. Chem. Symp. 12 (1978) 169.
[22] M.E. Casida, in: D.P. Chong (Ed.), Recent Advances in Density Functional Methods, Part I, World Scientific, Singapore, 1995, p. 155.
[23] A. Mukherji, M. Karplus, J. Chem. Phys. 38 (1963) 44.
[24] P.H. Dederichs, S. Blügel, R. Zeller, H. Akai, Phys. Rev. Lett. 53 (1984) 2512.
[25] D. Jayatilaka, D.J. Grimwood, Acta Crystallogr. A57 (2001) 76.
[26] D.J. Grimwood, D. Jayatilaka, Acta Crystallogr. A57 (2001) 87.
[27] I. Bytheway, D.J. Grimwood, D. Jayatilaka, Acta Crystallogr. A58 (2002) 232.
[28] I. Bytheway, D.J. Grimwood, B.N. Figgis, G.S. Chandler, D. Jayatilaka, Acta Crystallogr. A58 (2002) 244.
[29] D.J. Grimwood, I. Bytheway, D. Jayatilaka, J. Comput. Chem. 24 (2003) 470.
[30] A.M. Köster, J.U. Reveles, J.M. del Campo, J. Chem. Phys. 121 (2004) 3417.
[31] A. St-Amant, D.R. Salahub, Chem. Phys. Lett. 169 (1990) 387; Alain St-Amant, PhD Thesis, University of Montreal, 1992. M.E. Casida, C. Daul, A. Goursot, A. Köster, L.G.M. Pettersson, E. Proynov, A. St-Amant, D.R. Salahub principal authors, S. Crétien, H. Duarte, N. Godbout, J. Guan, C. Jamorski, M. Leboeuf, V. Malkin, O. Malkina, M. Nyberg, L. Pedocchi, F. Sim, A. Vela (contributing authors), computer code deMon-KS, version 3.5, deMon Software, 1988.
[32] M.E. Casida, C. Jamorski, E. Fadda, J. Guan, S. Hamel, D.R. Salahub, deMon-DynaRho version 3.2, University of Montreal and Université Joseph-Fourier, copyright, 2002.
[33] M.E. Casida, C. Jamorski, F. Bohr, J. Guan, D.R. Salahub, in: S.P. Karna, A.T. Yeates (Eds.), Theoretical and Computational Modeling of NLO and Electronic Materials Proceedings of ACS Symposium, Washington, DC, 1994, ACS Press, Washington, DC, 1996, p. 145.
[34] Andreas M. Koester, Patrizia Calaminici, Mark E. Casida, Roberto Flores, Gerald Geudtner, Annick Goursot, Thomas Heine, Andrei Ipatov, Florian Janetzko, Serguei Patchkovskii, J. Ulises Reveles, Alberto Vela, Dennis R. Salahub, deMon2k, Version 1.8, The deMon Developers, 2005.
[35] A.J. Sadlej, Collec. Czech. Chem. Commun. 53 (1988) 1995; A.J. Sadlej, Theor. Chim. Acta 79 (1992) 123; A.J. Sadlej, Theor. Chim. Acta 81 (1992) 45; A.J. Sadlej, Theor. Chim. Acta 81 (1992) 339.
[36] J. Andzelm, E. Radzio, D.R. Salahub, J. Comput. Chem. 6 (1985) 520.
[37] J. Andzelm, N. Russo, D.R. Salahub, J. Chem. Phys. 87 (1987) 6562.
[38] A. Herrmann, E. Schumacher, L. Wöste, J. Chem. Phys. 68 (1978) 2327.
[39] A. Modelli, G. Distefano, Z. Naturforsch. A 36 (1981) 1344.
[40] J. Guan, M.E. Casida, A.M. Köster, D.R. Salahub, Phys. Rev. B 52 (1995) 2184.
[41] P. Calaminci, K. Jug, A.M. Köster, J. Chem. Phys. 111 (1999) 4613.
[42] P. Calaminici, A.M. Köster, A. Vela, K. Jug, J. Chem. Phys. 113 (2000) 2199.
[43] L.G. Gerchikov, C. Guet, A.N. Ipatov, Phys. Rev. A 65 (2002) 13201.
[44] L.G. Gerchikov, C. Guet, A.N. Ipatov, Phys. Rev. A 66 (2003) 53202.
[45] L.G. Gerchikov, A.N. Ipatov, J. Phys. B 36 (2003) 1193.
[46] A.N. Ipatov, P.-G. Reinhard, E. Suraud, Int. J. Mol. Sci. 4 (2003) 300.
[47] A.N. Ipatov, P.-G. Reinhard, E. Suraud, Eur. Phys. J. D 30 (2004) 65.
[48] B. Gervais, E. Giglio, E. Jacquet, A. Ipatov, P.-G. Reinhard, F. Fehrer, E. Suraud, Phys. Rev. A 71 (2005) 015201.
[49] B. Gervais, E. Giglio, E. Jacquet, A. Ipatov, P.-G. Reinhard, E. Suraud, J. Chem. Phys. 121 (2004) 8466.
[50] A. Ipatov, L. Gerchikov, C. Guet, J. Comp. Mater. Sci., in press.
[51] L.G. Gerchikov, C. Guet, A.N. Ipatov, Isr. J. Chem. 44 (2004) 205.
[52] C. Jamorski, J.B. Foresman, C. Thilgen, H.-P. Lüthi, J. Chem. Phys. 116 (2002) 8761.
[53] C. Jamorski Jödicke, H.P. Lüthi, J. Chem. Phys. 117 (2002) 4146.
[54] C. Jamorski Jödicke, H.P. Lüthi, J. Chem. Phys. 117 (2002) 4157.
[55] C. Jödicke Jamorski, H.-P. Lüthi, J. Chem. Phys. 119 (2003) 12852.
[56] C. Jamorski Jödicke, H.-P. Lüthi, J. Am. Chem. Soc. 125 (2003) 252.
[57] C. Jamorski Jödicke, H.-P. Lüthi, Chem. Phys. Lett. 368 (2003) 561.
[58] C. Jödicke Jamorski, M.E. Casida, J. Phys. Chem. B 108 (2004) 7132.
[59] W.A. de Heer, Rev. Mod. Phys. 65 (1993) 611.
[60] U. Kaldor, Isr. J. Chem. 31 (1991) 345.
[61] M. Gross, F. Spiegelmann, J. Chem. Phys. 108 (1998) 4148.
[62] A. Henriet, F. Masnou-Seeuws, J. Phys. B 20 (1987) 671.
[63] D.W. Davies, G.J.R. Jones, Chem. Phys. Lett. 81 (1981) 279.
[64] C.R.C. Wang, S. Pollack, D. Cameron, M. Kappes, J. Chem. Phys. 93 (1990) 3789.
[65] V. Bonačić-Koutecký, P. Fantucci, J. Koutecký, J. Chem. Phys. 96 (1990) 7938.
[66] P.P. Prasad, D.J. Williams, Introduction to Nonlinear Optical Effects in Molecules and Polymers, Wiley, New York, 1991.
[67] F. Gutierrez, PhD Thesis, Université Paul Sabatier, Toulouse, France, 2002.
[68] L. Serrano-Andres, M. Merchán, B.O. Roos, R. Lindh, J. Am. Chem. Soc. 117 (1995) 3189.
[69] A. Germain, PhD Thesis, Univeristé de Paris Sud, Orsay, France, 1996.